The Myth of Laboratory Two-Dimensional Wall-Bounded Turbulent Flows

Ricardo Vinuesa[1]

Advisor: Hassan M. Nagib[1]
Co-Advisors: Philipp Schlatter[2] and Paul F. Fischer[3]

[1]Illinois Institute of Technology (IIT), USA.
[2]Royal Institute of Technology (KTH), Sweden.
[3]Argonne National Laboratory (ANL), USA.

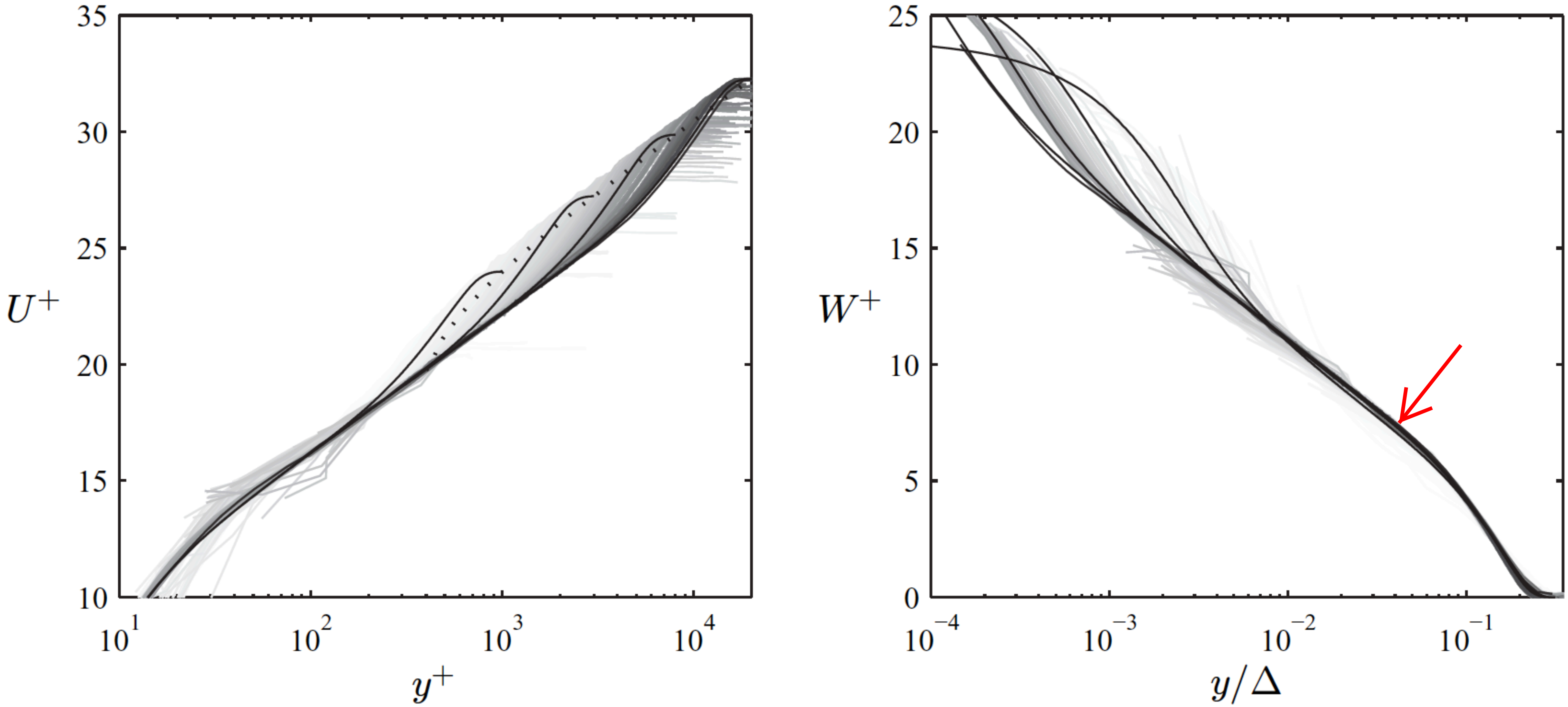

(a) U^+ versus y^+ (b) W^+ versus y/Δ

Figure 6. Variation of experimental mean-velocity profiles with Reynolds number in inner and outer scalings. Only profiles that meet the Π and H criteria are shown. Profiles with increasing Re are shown in progressively darker shades of gray. Also shown is the composite velocity profile for $\delta^+ = 1000$, 3000, 8000 and 20 000. · · · · ·: evolution of $2\Pi/\kappa$ relative to the log-law.

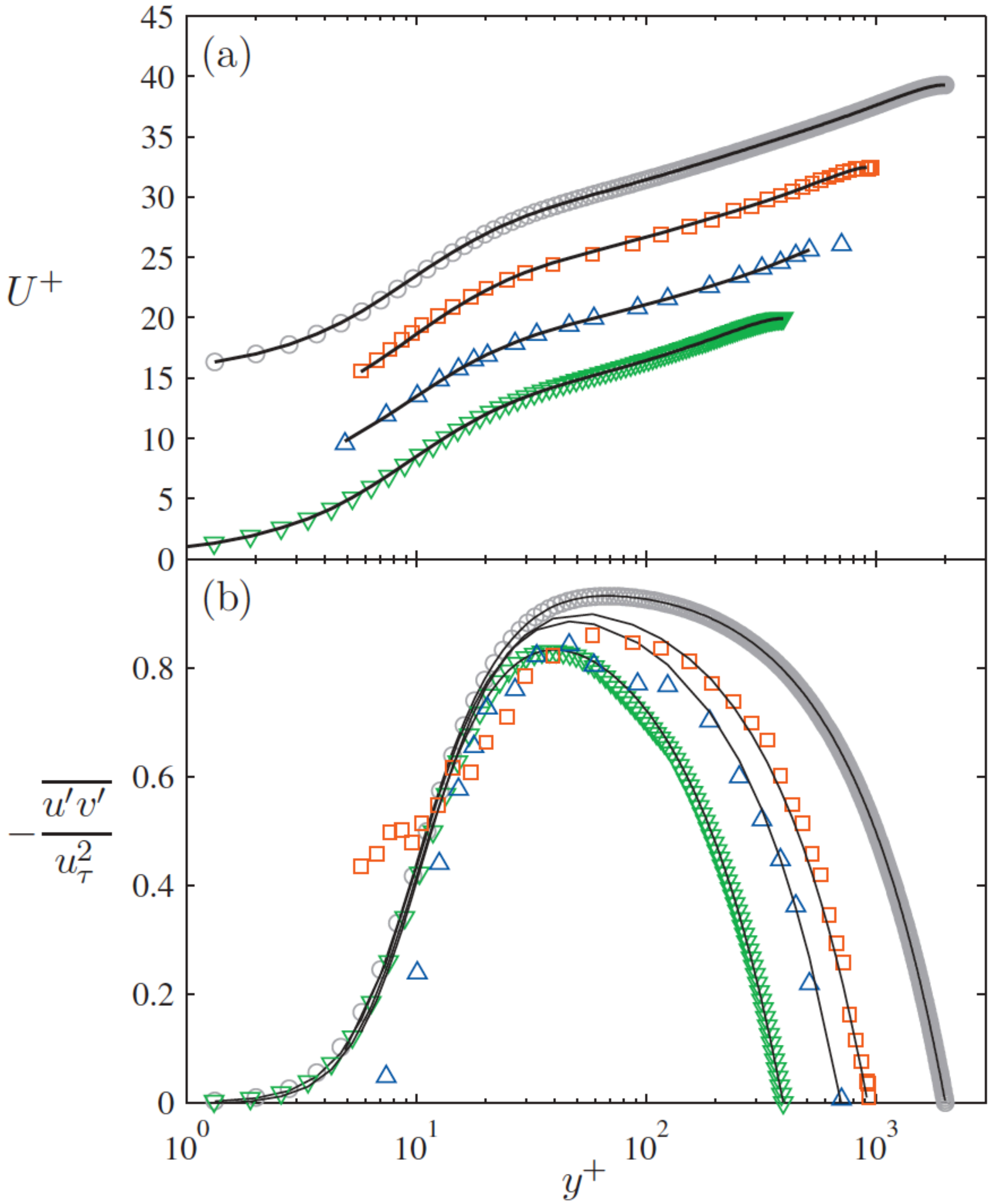

FIG. 1. (Color) Comparison of fitted composite profile with channel flow data in inner scaling. (a) U^+ vs y^+. Note the upward shift in profiles by five units with increasing Reynolds numbers. (b) $-\overline{u'v'}^+$ vs y^+. Symbols indicate the following: (gray ○) Jiménez *et al.* (Ref. 21), $\mathrm{Re}_\tau=2003$; (red □) Niederschulte *et al.* (Ref. 12), $\mathrm{Re}_\tau=921$; (blue △) Wei and Willmarth (Ref. 11), $\mathrm{Re}_\tau=706$; and (green ▽) Kim *et al.* (Ref. 18), $\mathrm{Re}_\tau=395$. Solid line represents the fitted composite profile.

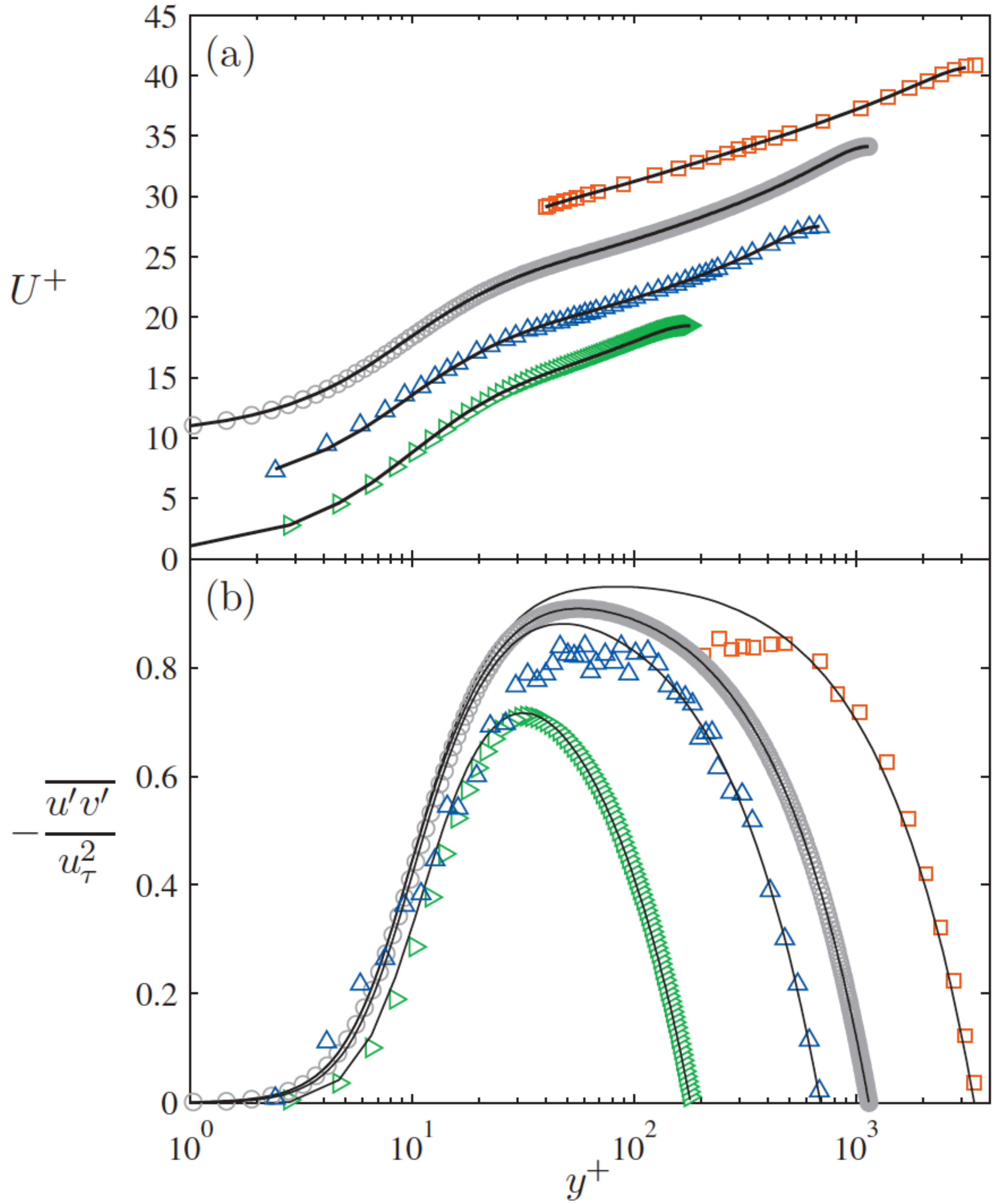

FIG. 2. (Color) Comparison of fitted composite profile with pipe flow data in inner scaling. (a) U^+ vs y^+. Note the upward shift in profiles by five units with increasing Reynolds numbers. (b) $-\overline{u'v'}^+$ vs y^+. Symbols indicate the following: (red □) Perry *et al.* (Ref. 8), $\mathrm{Re}_\tau=3408$; (gray ○) Wu and Moin (Ref. 17), $\mathrm{Re}_\tau=1141$; (blue △) den Toonder and Nieuwstadt (Ref. 10), $\mathrm{Re}_\tau=690$; and (green ▷) Eggels *et al.* (Ref. 15), $\mathrm{Re}_\tau=180$. Solid line represents the fitted composite profile.

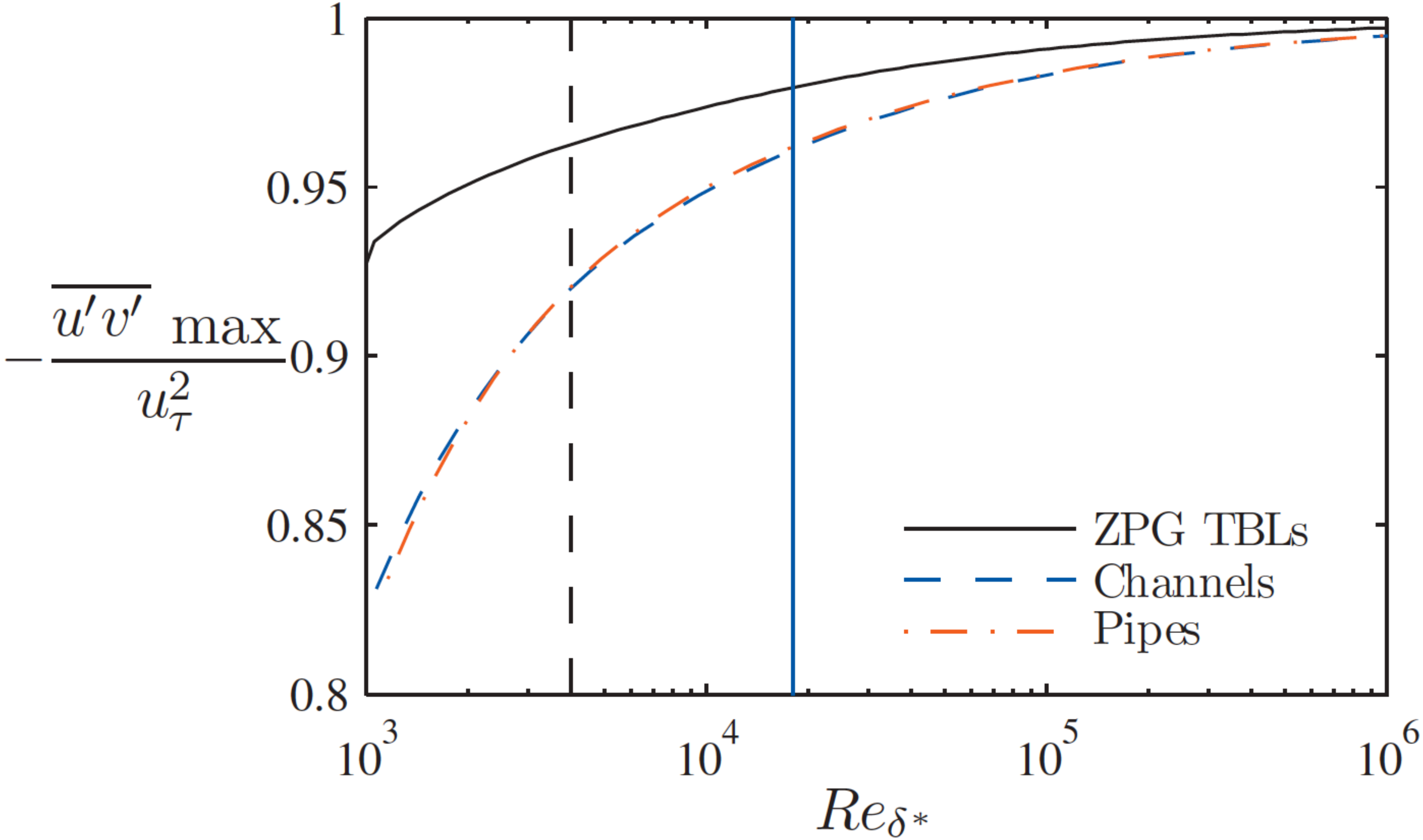
1
0.95
0.9
0.85
0.8
$-\frac{\overline{u'v'}\ \max}{u_\tau^2}$
10^3
10^4
10^5
10^6
Re_{δ^*}
ZPG TBLs
Channels
Pipes

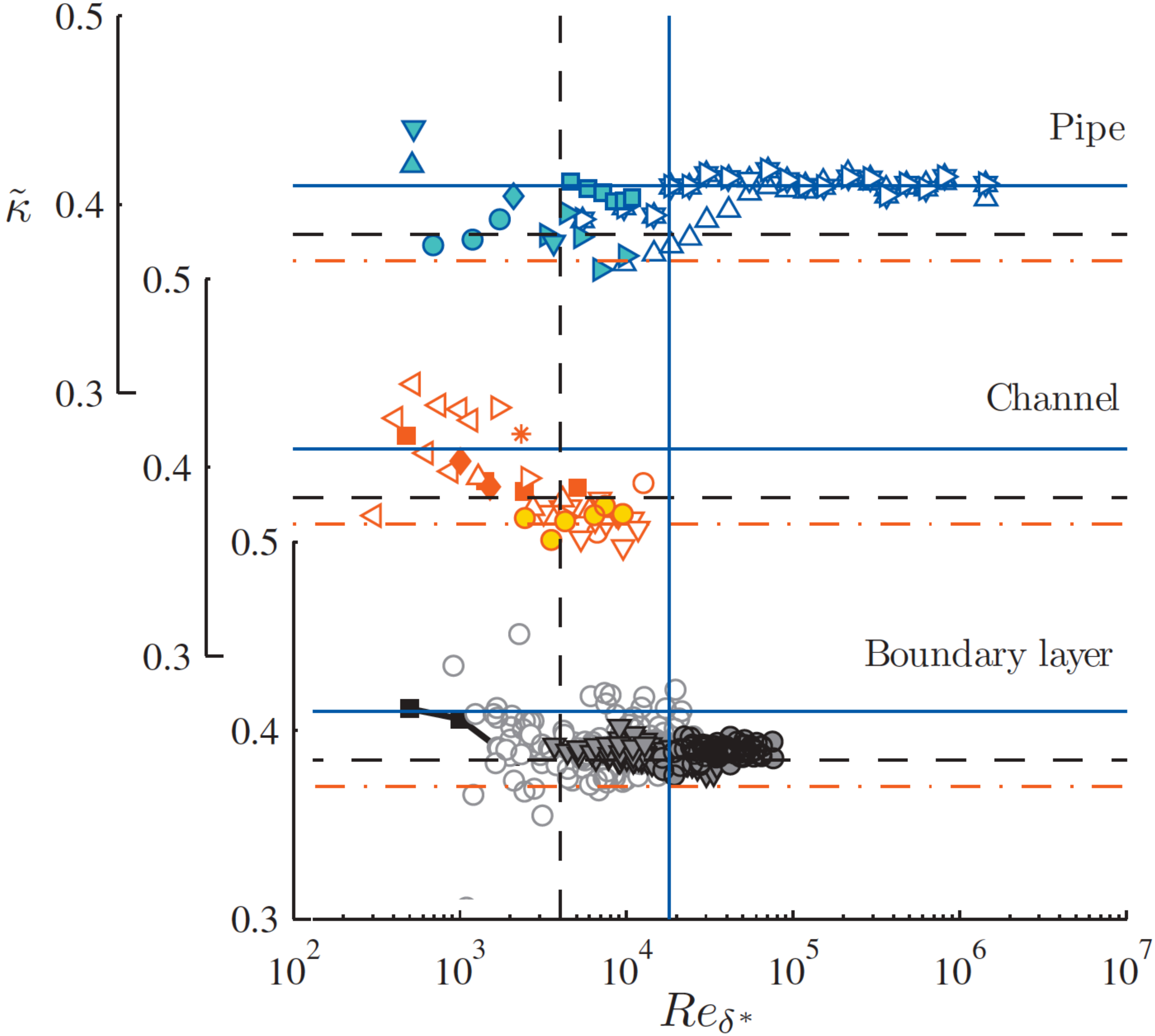
Pipe
Channel
Boundary layer
$\tilde{\kappa}$
0.5
0.4
0.3
10^2
10^3
10^4
10^5
10^6
10^7
Re_{δ^*}

Asymptotic value of κ for channel flows

- It is not possible to obtain the **asymptotic** κ for channel flows by analyzing the velocity profiles: the **overlap region** is not large enough to isolate the **inner-outer interaction**.
- The overlap region can be described in **inner** and **outer** variables:

$$\left.\begin{aligned} U^+ &= \frac{1}{\kappa}\ln(y^+) + B \\ U^+ - U_c^+ &= \frac{1}{\kappa}\ln(y/h) + A \end{aligned}\right\} \Rightarrow U_c^+ = \frac{1}{\kappa}\ln(Re_\tau) + C$$

- This **skin friction relation** combines the **inner** and **outer** descriptions of the overlap region $\Rightarrow$ It is possible to obtain the **asymptotic** κ, even if the “high-Re” conditions have not been achieved.
- No velocity profiles are used in this analysis: only the **centerline velocity** (U_c), and the **length scales** from the **inner** (ν/u_τ) and **outer** (h) regions are required.

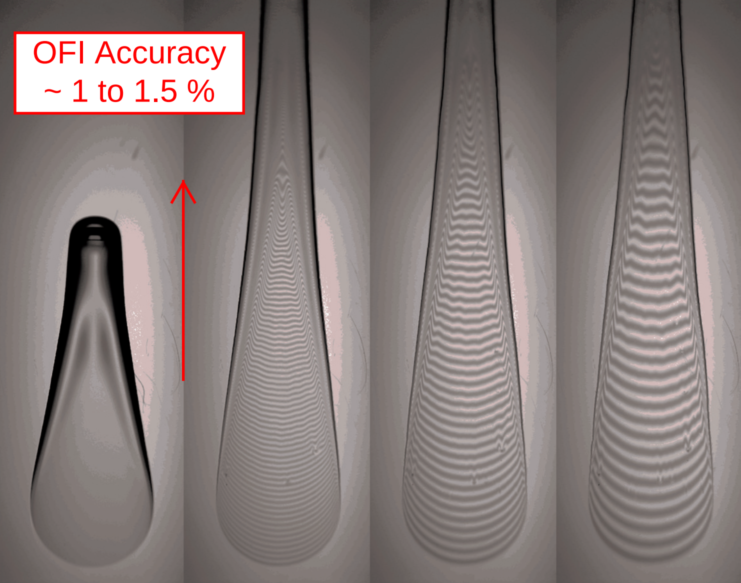
OFI Accuracy
~ 1 to 1.5 %

Asymptotic value of κ for channel flows

- Approach used by Monkewitz *et al.* (2008) for **ZPF boundary layers** $\Rightarrow$ Red line is a power law prediction, but experimental data show $\kappa = 0.384$ from $Re_\tau \simeq 200$.

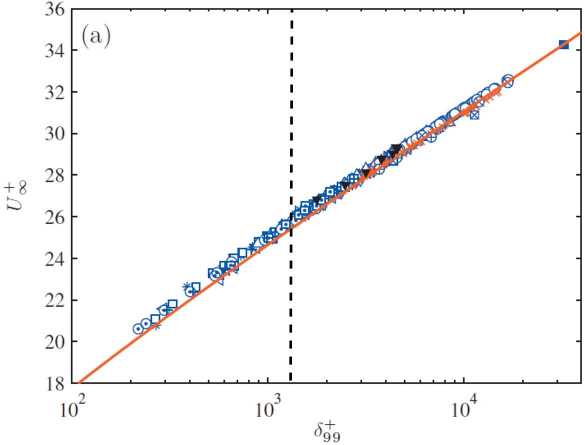

Aspect ratio configurations

- Four **access ports** were used for velocity and wall shear measurements in a selection of **aspect ratio cases** ranging from 12.8 to 48.
- Different **channel heights** H lead to various **normalized distances from entrance** x/H:

Plug location	$\mathrm{AR} =$ 12.8, 14.4 & 19.2	$\mathrm{AR} =$ 18 & 24	$\mathrm{AR} = 24 - 3$	$\mathrm{AR} = 24 - 2$ & 32	$\mathrm{AR} = 48$
1.52 m	96	120	135	160	**240**
2.12 m	134	167	188	**223**	**334**
2.74 m	173	**216**	**243**	**288**	**432**
3.35 m	**211**	**264**	**297**	**352**	**528**
3.66 m	**231**	**288**	**324**	**384**	**576**

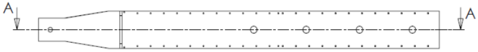

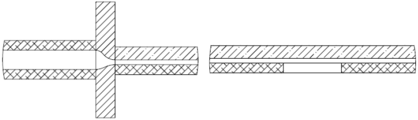

Measurement techniques III

- **Static pressure measurements:** A total of **37 static pressure ports** were used to measure the pressure drop along the channel with respect to the reference static pressure from the Pitot tube.
- A Setra 2204 **differential pressure transducer** is connected to a **Scanivalve** and the **reference port**. Each port is read for 20 s at a sampling rate of 1000 Hz for ΔP.
- **Streamwise pressure drop** at centerline is widely used to estimate wall shear $\Rightarrow$ **Not a local measure of τ_w !!**

$$\tau_{w,\mathrm{PG}} = -\frac{H}{2}\frac{dP}{dx}.$$

- **No spanwise variation** of ΔP was observed $\Rightarrow$ Signature of three-dimensional effects not reflected in static pressure.

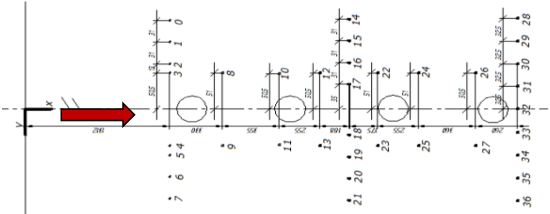

Wall shear measurements

- Local measurements of skin friction coefficient $C_{f,c} = 2(u_\tau/U_c)^2$ with OFI for $x/H > 200$ reveal a **decreasing wall shear** trend up to **AR = 24**.
- Measurements of $C_{f,c}$ obtained from streamwise **pressure gradient do not show the same trend**, and only match OFI at the lowest aspect ratio.

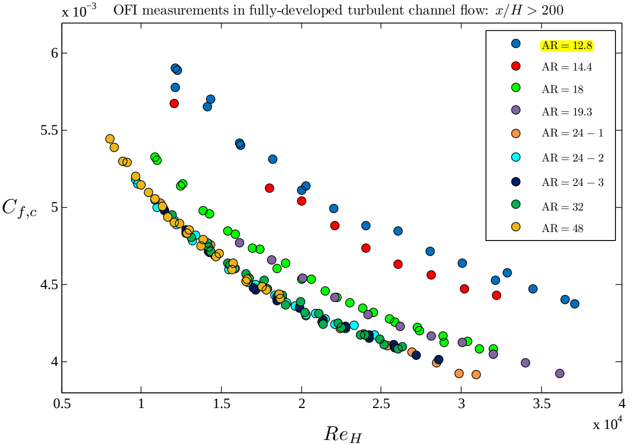

Wall shear measurements

- Local measurements of skin friction coefficient $C_{f,c} = 2(u_\tau/U_c)^2$ with OFI for $x/H > 200$ reveal a **decreasing wall shear** trend up to **AR** $=$ **24**.
- Measurements of $C_{f,c}$ obtained from streamwise **pressure gradient do not show the same trend**, and only match OFI at the lowest aspect ratio.

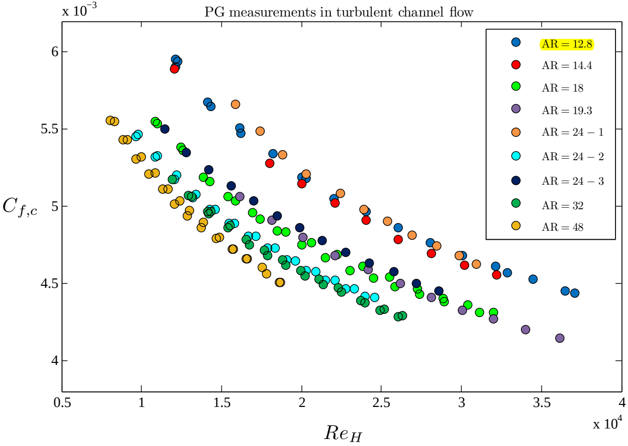

High-*Re* von Kármán coefficient κ

- Local measurements of wall shear on a **high-AR ($\geq$ 24) fully-developed (x $>$ 200H)** turbulent duct flow can be used to obtain the **high-Re von Kármán coefficient** $\kappa \Rightarrow \mathbf{1}/\kappa \ln(\mathbf{Re}_\tau) + \mathbf{C}$:

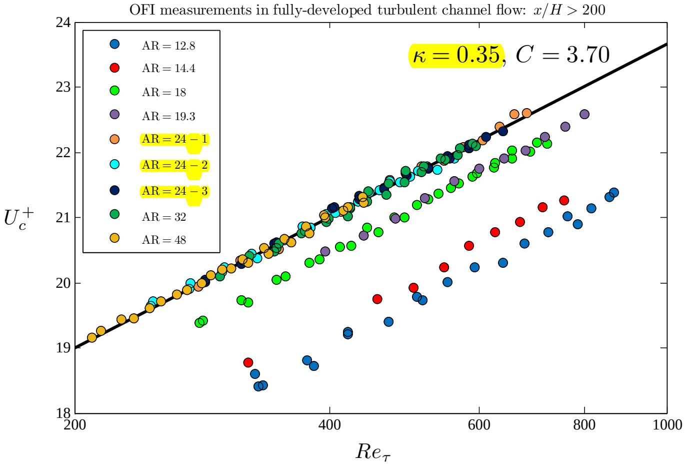

Comparison with other data available in the literature

- DNSs of **z-periodic channels** yield a κ value of 0.39 $\Rightarrow$ **not same flow**.
- Zanoun *et al.* (2003) performed OFI measurements in an $\mathrm{AR} = 12$ duct at $x/H = 115$ $\Rightarrow$ **Different** κ when looking at low-*Re*, high-*Re* or all data combined.

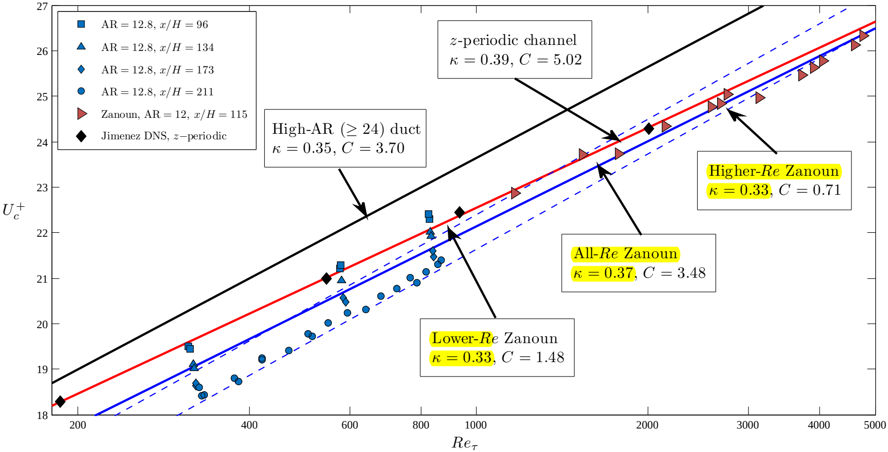

Aim of the computations

- Conditions given by $z-$periodic **channel flow** DNSs **cannot be reproduced experimentally** $\Rightarrow$ What are the **physical mechanisms** present in a **duct** and not captured by the **channel**?

- **Three-dimensional effects present in the duct:**
  i) **Side-wall boundary layers**: They accelerate the irrotational core of the duct, **increasing** wall shear.
  $\Rightarrow$ **Energy flux from side-walls to duct centerplane**.
  ii) **Secondary motions of Prandtl's second kind:** They convect mean velocity from the walls to the corner bisectors, thus **reducing** wall shear.
  $\Rightarrow$ **Energy flux from duct centerplane to side-walls**.

Secondary motions

- Secondary motions refer to the **mean cross-stream flow** V, W, normal to the streamwise direction x.
- Prandtl's **first kind** are associated with vortex stretching and tilting terms.
  $\Rightarrow$ **Not present** in fully-developed ducts.
- Prandtl's **second kind** are associated with the **secondary shear stress** $\overline{vw}$ and the **anisotropy of the cross-stream stress** $\overline{v^2} - \overline{w^2}$.

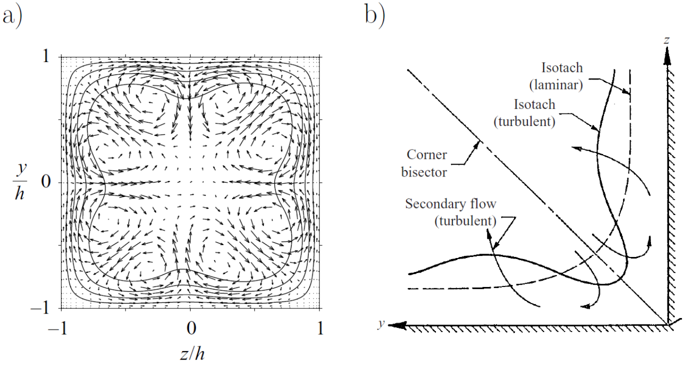

Numerical code: **Nek5000**

- Developed by Fischer *et al.* at Argonne National Laboratory (**ANL**) in 2008.
- Based on Spectral Element Method (**SEM**) by Patera (1984).
- Navier-Stokes cast in weak form, and discretized in space through **Galerkin** approximation.
- **Nonlinear** terms are treated **explicitly** (EXT3), and **viscous** terms **implicitly** (BDF3).
- $\mathbb{P}_N - \mathbb{P}_{N-2}$ formulation for **velocity** and **pressure**.
- Three-dimensional velocity vector is interpolated within a spectral element by means of three **Lagrange polynomials** of order N.
- Gauss-Lobatto-Legendre (**GLL**) quadrature points within a spectral element and **Modified Gauss-Lobatto-Chebyshev** distribution of elements.

Characteristics of the simulations I

- **Computations** carried out at three supercomputing facilities:
  i) Cray XE6 machine **Lindgren** at the PDC center from KTH, Stockholm.
  ii) Blue Gene/P machine **Intrepid** at the ALCF from Argonne National Lab.
  iii) Cray XT5 machine **Louhi** at the CSCIT center for Science in Espoo, Finland.
- High-order interpolation ($\mathbf{N} = 11$) within spectral elements.
- Box length $\mathbf{L_x} = \mathbf{25h}$ in all cases:

AR	$Re_{\tau,c}$	Re_b	$Re_{b,c}$	Grid-points	ETT^*_S	ETT^*_A	ε
1	178	2500	2796	28 million	30	1602	1.08×10^{-3}
3	178	2581	2786	62 million	58	460	2.95×10^{-4}
5	176	2592	2775	96 million	28	280	3.46×10^{-4}
7	174	2575	2737	130 million	28	155	1.28×10^{-3}
10	–	–	–	185 million	–	–	–
1	323	5086	5604	145 million	26.5	112	8.87×10^{-4}
3	–	–	–	370 million	–	–	–

Characteristics of the simulations II

- Nek5000 Highly accurate, scales up to $\mathbf{10^6}$ cores.
- Part of the **data processing** and preliminary **LES simulations** performed at Dell computational cluster **Andrea** at IIT, Chicago, USA.
- Mesh resolution:
  i) Homogeneous x direction: $\Delta x^+_{\max} < 10$.
  ii) Core of inhomogeneous y and z directions: $\Delta y^+_{\max} < 5$.
  iii) Near-wall region: $\simeq 7$ points below 1^+.
- Re_b is **adjusted** iteratively to keep $\mathbf{Re_{b,c}}$ **fixed** with AR.
  $\Rightarrow$ Emulate **experiment** and compare with **reference** $z-$periodic channel.
- Preliminary **low-resolution** runs with $N = 5$ and $N = 7$ to approach **fully-developed turbulence.**

Numerical tripping

- Tripping is implemented as a random **wall-normal** volume force. Spanwise **line** with fixed **amplitude**, **spanwise length scale** and **temporal frequency**.

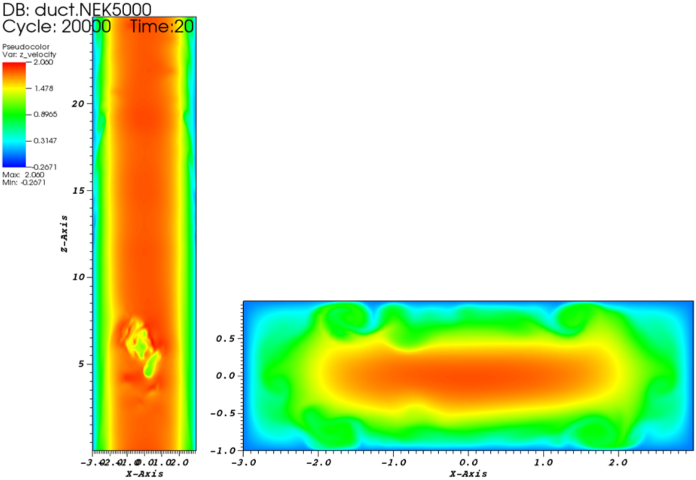

Numerical tripping

- Tripping is implemented as a random **wall-normal** volume force. Spanwise **line** with fixed **amplitude**, **spanwise length scale** and **temporal frequency**.

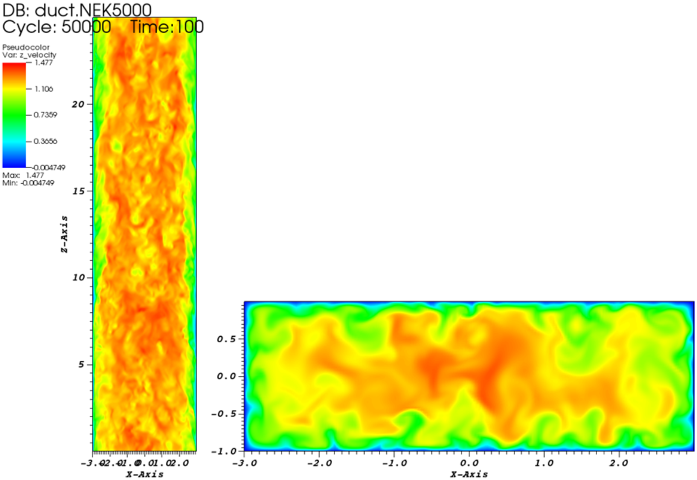

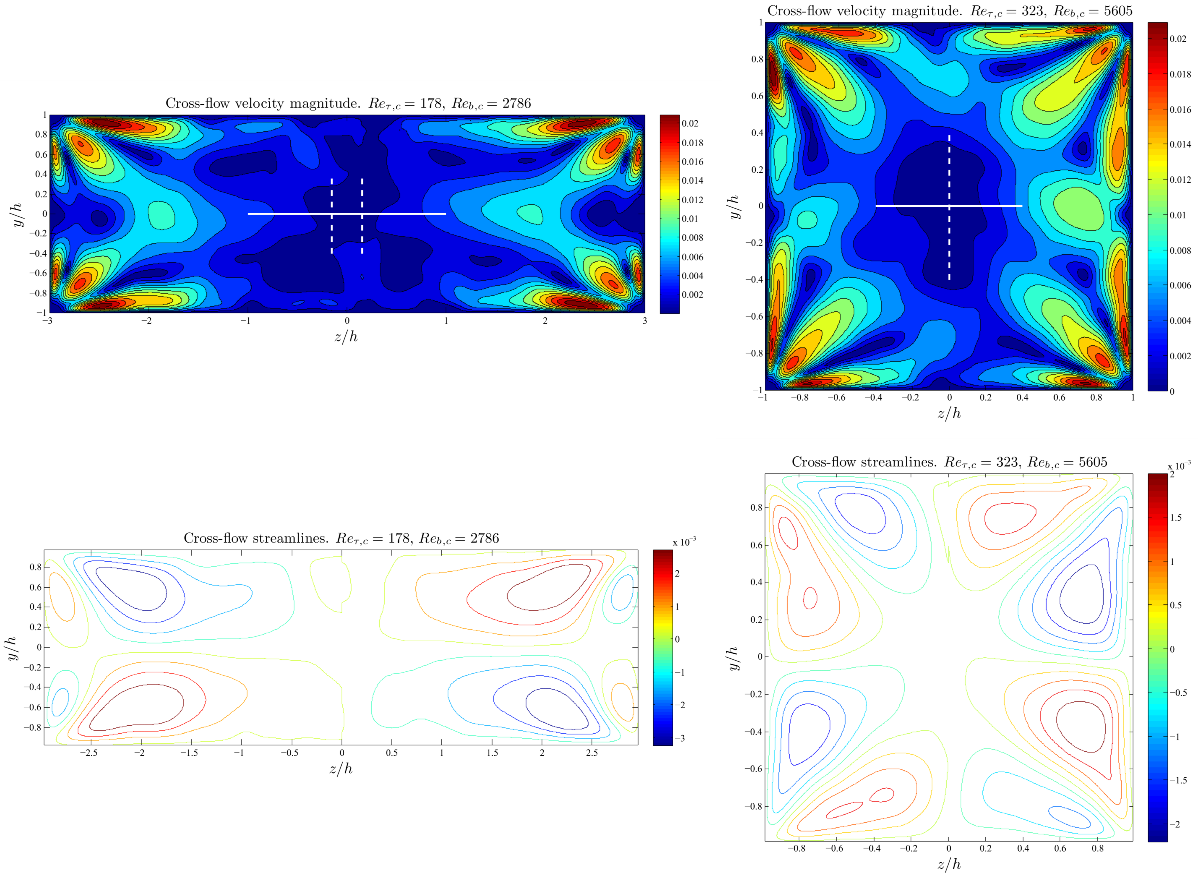

Figure 3. Cross-flow velocity magnitude $\sqrt{V^2+W^2}$ (top) and contours of the streamfunction (bottom) for the AR $= 3$ duct case computed at $Re_{\tau,c} \simeq 180$ (left) and the AR $= 1$ duct case with $Re_{\tau,c} \simeq 330$. Solid white lines represent the upper and lower boundary layer thicknesses at $z = 0$, $\delta_y \simeq h$. Dashed white lines show the side-wall boundary layer thicknesses at $y = 0$, $\delta_z \simeq 2.85h$ (left) and $\delta_z \simeq h$ (right).

Comparison with OFI measurements

- Evolution of wall shear with aspect ratio is **different for low-ARs**:
  - i) AR $= 1 \Rightarrow 3$: Skin friction **increases**.
  - ii) AR $= 3 \Rightarrow 5 \Rightarrow 7$: Skin friction **decreases**.

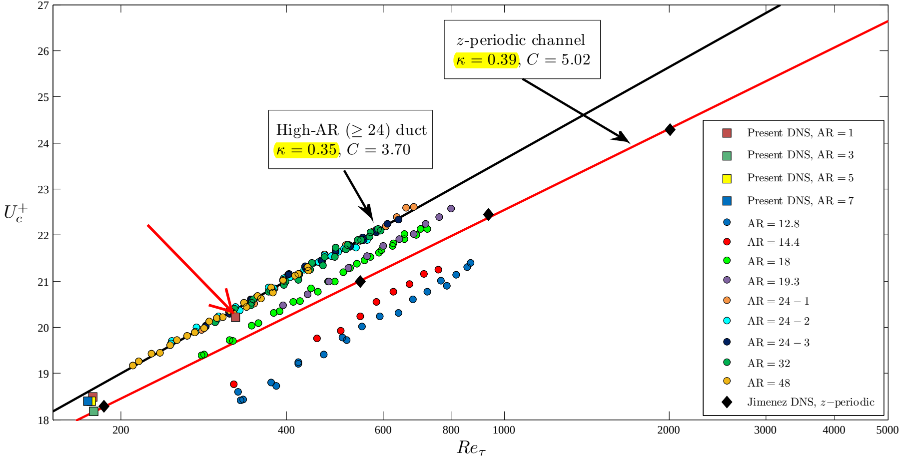

Description of AR trend

- Evolution of skin friction with AR in the low-AR range can be explained in terms of **side-wall boundary layers** and **secondary motions**.

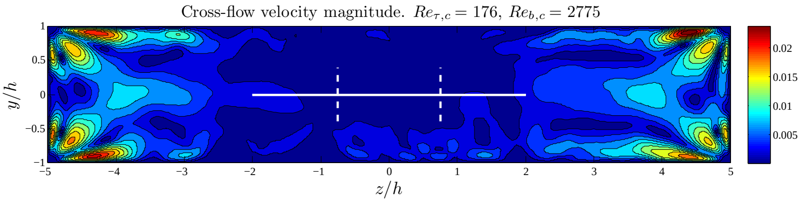

Description of AR trend

- Evolution of skin friction with AR in the low-AR range can be explained in terms of **side-wall boundary layers** and **secondary motions**.

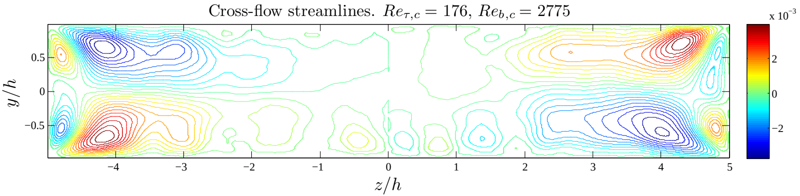

Description of AR trend

- Evolution of skin friction with AR in the low-AR range can be explained in terms of **side-wall boundary layers** and **secondary motions**.

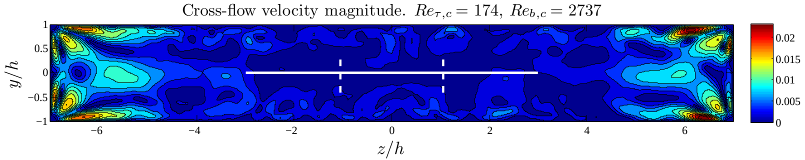

Description of AR trend

- Evolution of skin friction with AR in the low-AR range can be explained in terms of **side-wall boundary layers** and **secondary motions**.

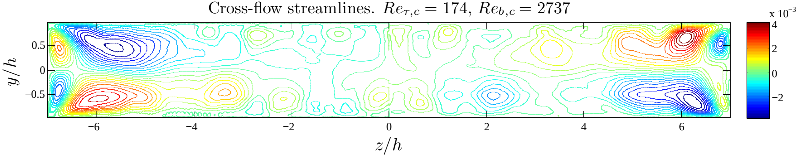

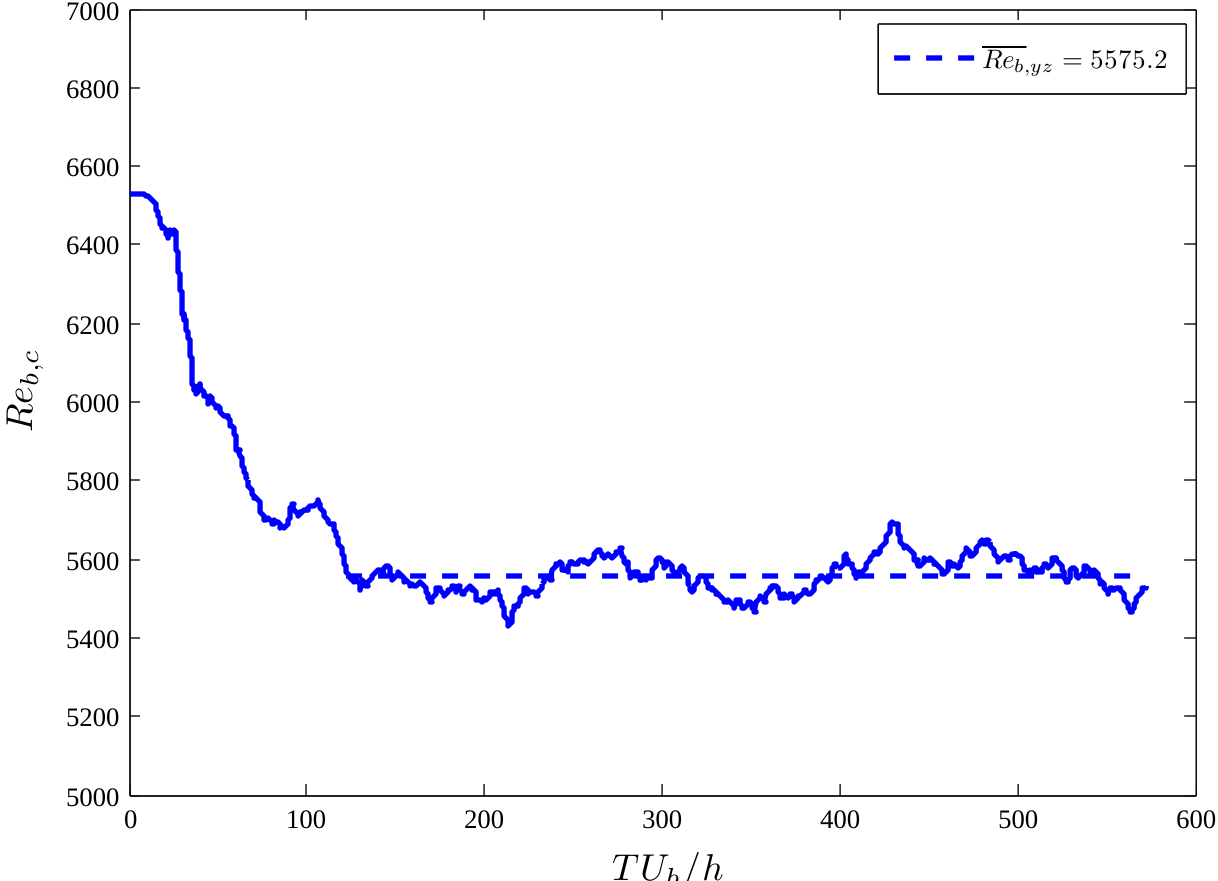

$\overline{Re_{b,yz}} = 5575.2$
7000
6800
6600
6400
6200
6000
5800
5600
5400
5200
5000
$Re_{b,c}$
0
100
200
300
400
500
600
TU_b/h

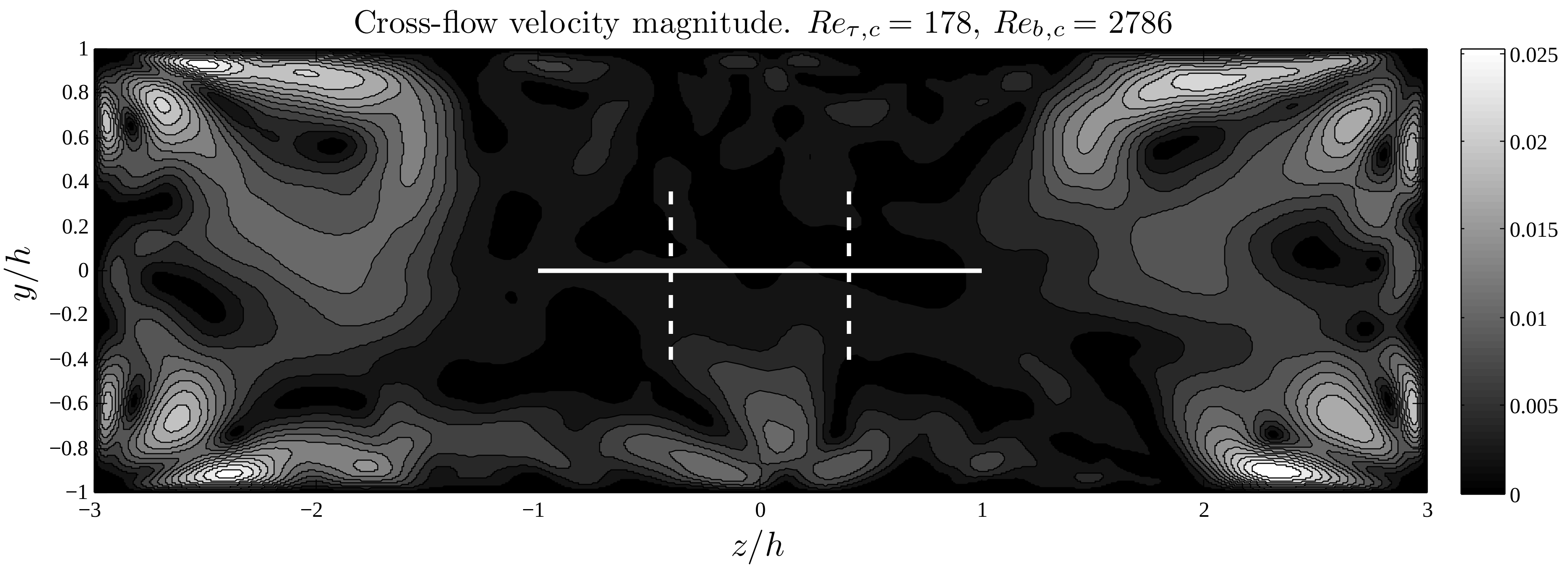

Cross-flow velocity magnitude. $Re_{\tau,c} = 178$, $Re_{b,c} = 2786$
y/h
z/h
1
0.8
0.6
0.4
0.2
0
−0.2
−0.4
−0.6
−0.8
−1
−3
−2
−1
0
1
2
3
0.025
0.02
0.015
0.01
0.005
0

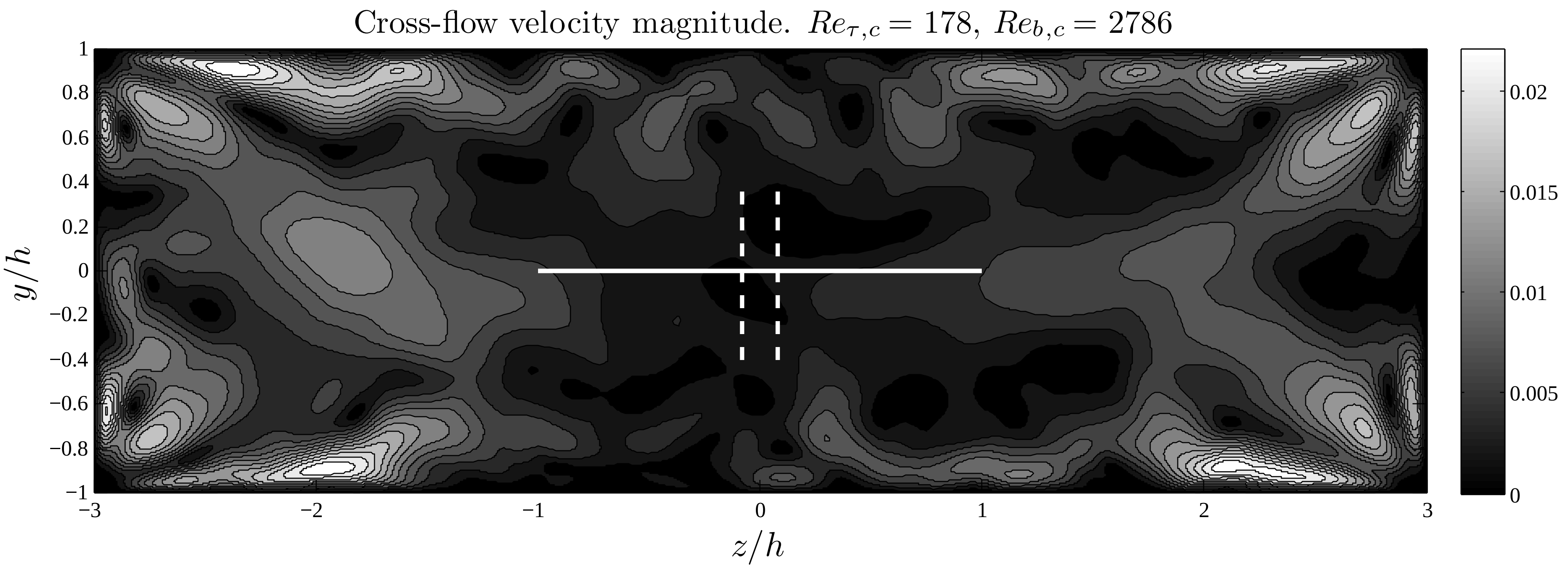

Cross-flow velocity magnitude. $Re_{\tau,c} = 178$, $Re_{b,c} = 2786$
y/h
z/h
1
0.8
0.6
0.4
0.2
0
−0.2
−0.4
−0.6
−0.8
−1
−3
−2
−1
0
1
2
3
0.02
0.015
0.01
0.005
0

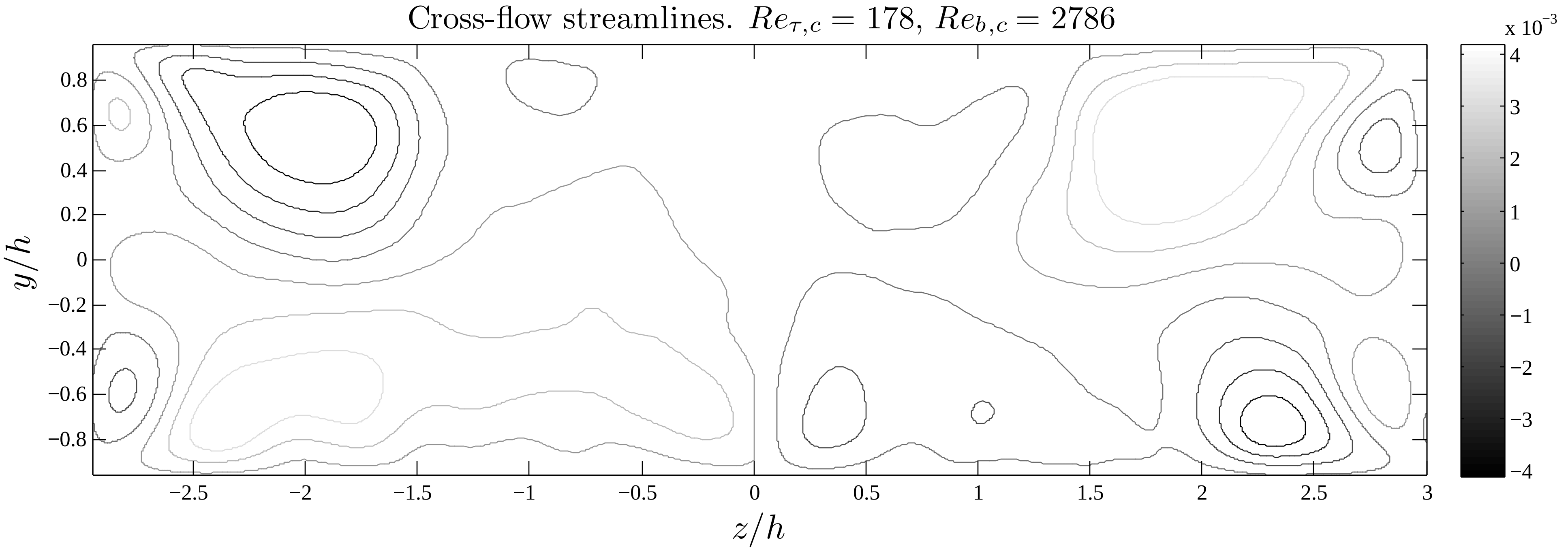

Cross-flow streamlines. $Re_{\tau,c} = 178$, $Re_{b,c} = 2786$
y/h
z/h
0.8
0.6
0.4
0.2
0
−0.2
−0.4
−0.6
−0.8
−2.5
−2
−1.5
−1
−0.5
0
0.5
1
1.5
2
2.5
3
x 10^{-3}
4
3
2
1
0
−1
−2
−3
−4

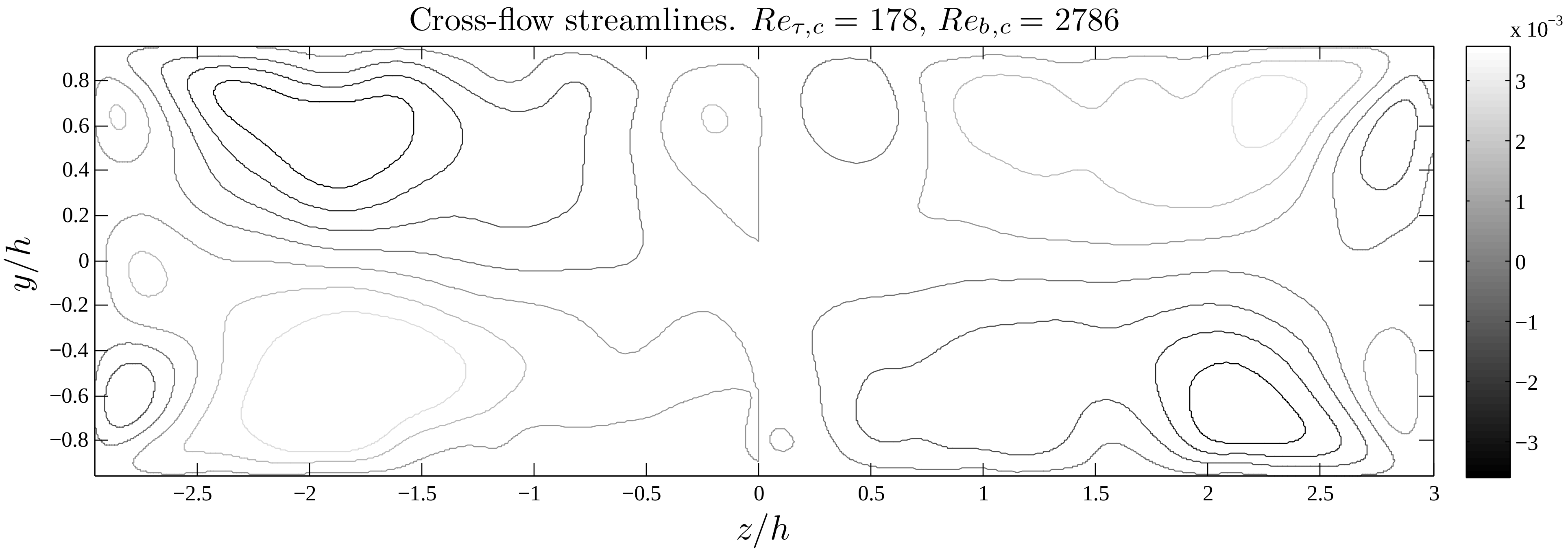

Cross-flow streamlines. $Re_{\tau,c} = 178$, $Re_{b,c} = 2786$
x 10^{-3}
3
2
1
0
−1
−2
−3
0.8
0.6
0.4
0.2
0
−0.2
−0.4
−0.6
−0.8
y/h
−2.5
−2
−1.5
−1
−0.5
0
0.5
1
1.5
2
2.5
3
z/h

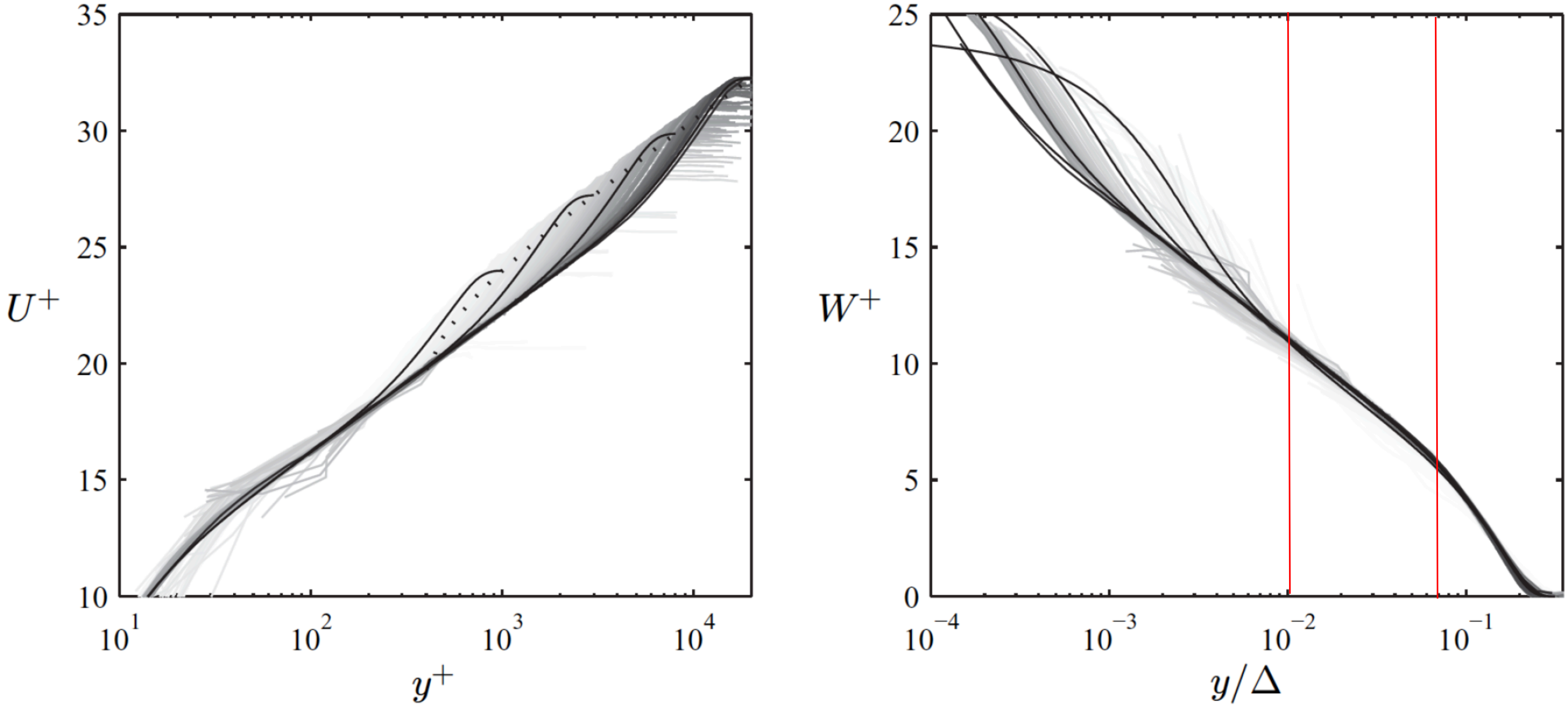

(a) U^+ versus y^+ (b) W^+ versus y/Δ

Figure 6. Variation of experimental mean-velocity profiles with Reynolds number in inner and outer scalings. Only profiles that meet the Π and H criteria are shown. Profiles with increasing Re are shown in progressively darker shades of gray. Also shown is the composite velocity profile for $\delta^+ = 1000$, 3000, 8000 and 20 000. $\cdot\cdot\cdot\cdot\cdot$: evolution of $2\Pi/\kappa$ relative to the log-law.

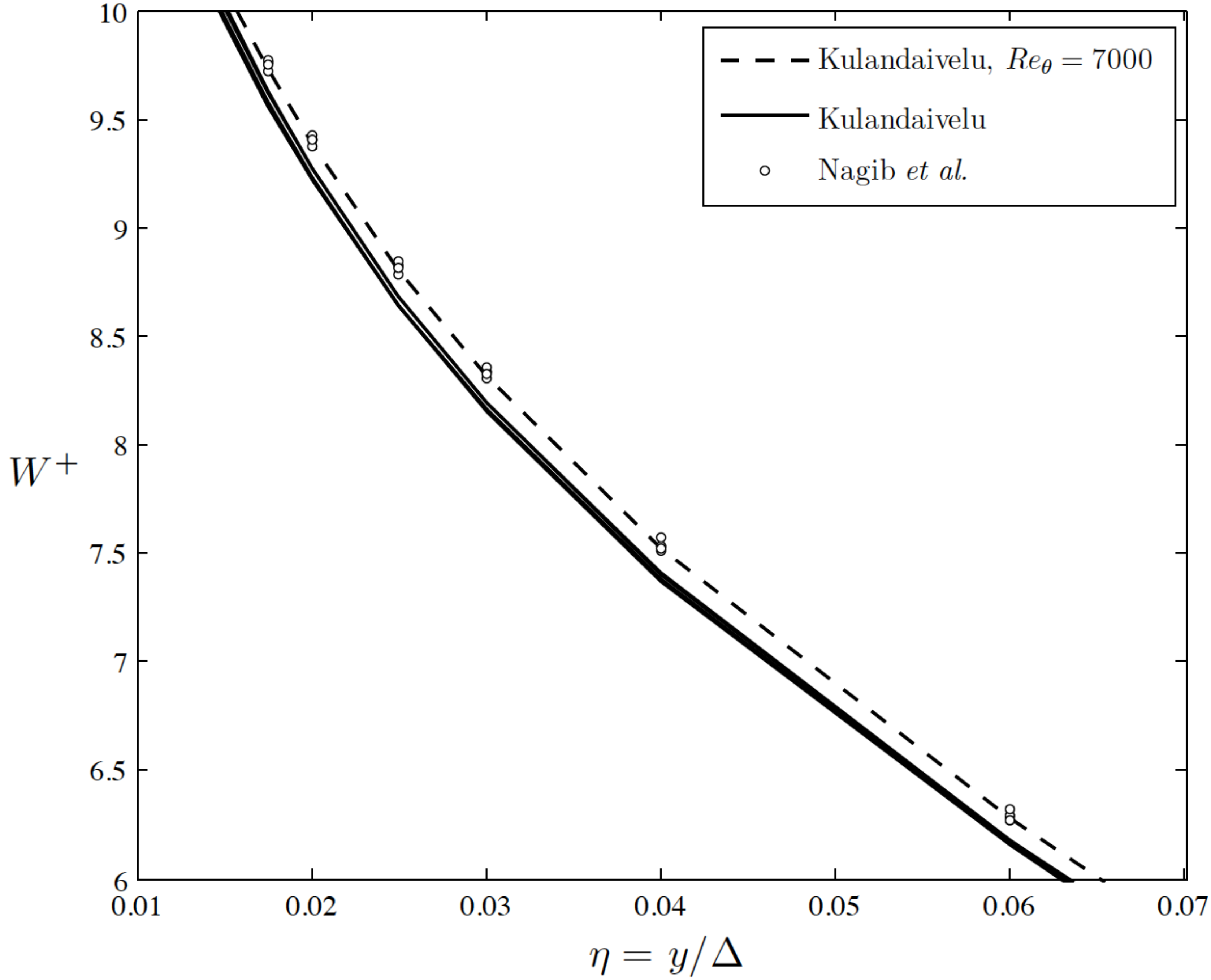

Figure 4.3. Comparison of velocity defect profiles in outer scaling (using the Clauser boundary layer thickness $\Delta = U_\infty^+ \delta^*$) for ZPG TBL measurements by Kulandaivelu [43] and Nagib *et al.* [44].

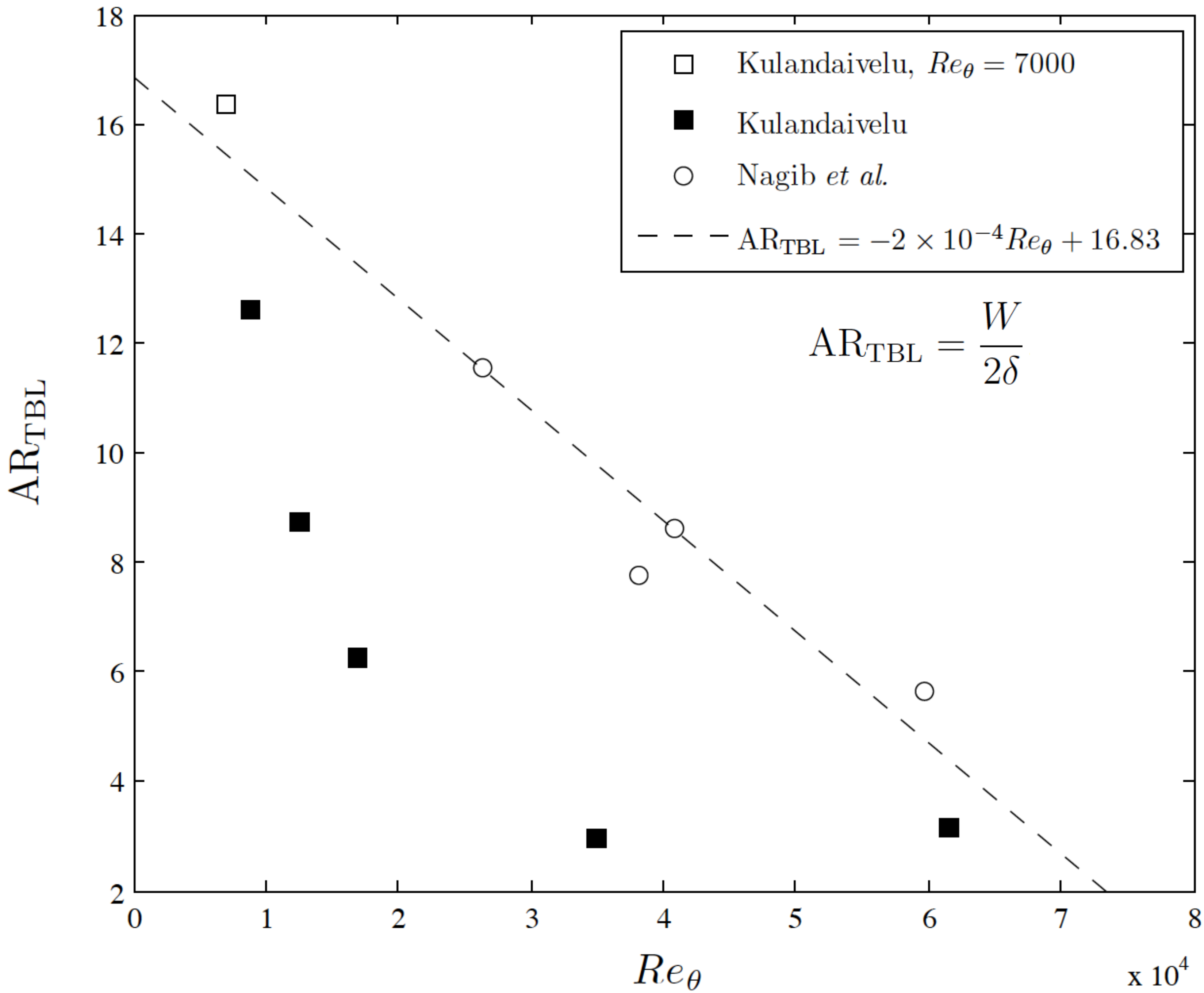

Figure 4.4. Equivalent TBL aspect ratio from runs by Kulandaivelu [43] and Nagib *et al.* [44]. Linear fit to cases showing good agreement in Figure 4.3 also presented.

Aspect ratio 5, $Re_{\tau,c} = 176$

- Comparison of duct spanwise profiles, duct centerplane and turbulent channel by Moser *et al.* at $Re_b \simeq 2800$.

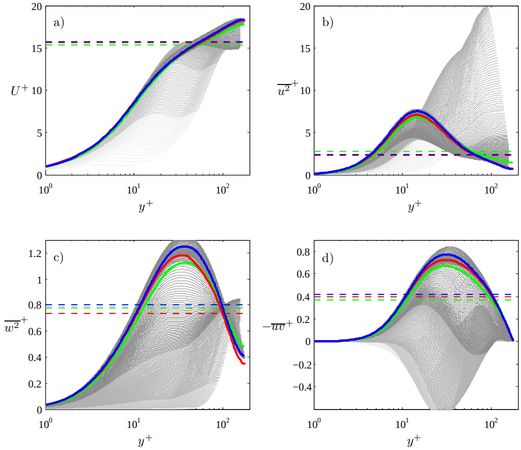

Aspect ratio 1, $Re_{\tau,c} = 178$

- Coherent vortices obtained using the **Q criterion**:

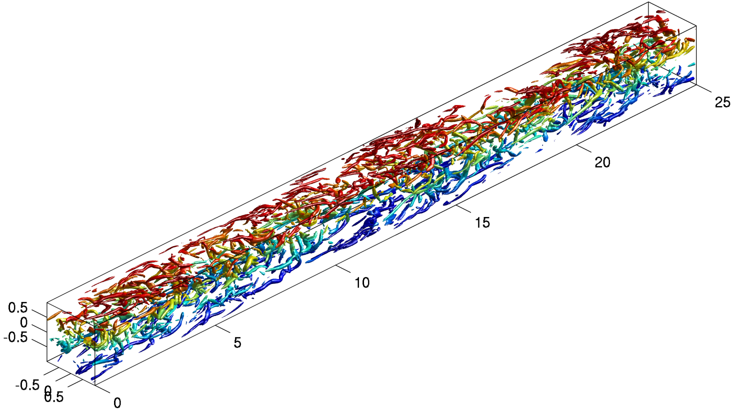

Aspect ratio 5, $Re_{\tau,c} = 176$

- Coherent vortices obtained using the **Q criterion**:

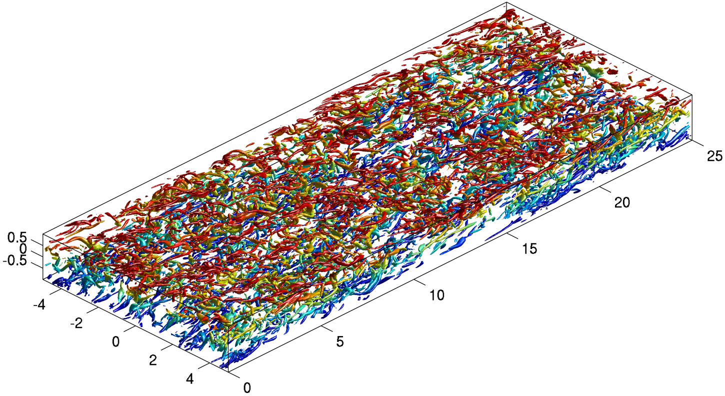

Aspect ratio 7, $Re_{\tau,c} = 174$

- Coherent vortices obtained using the **Q criterion**:

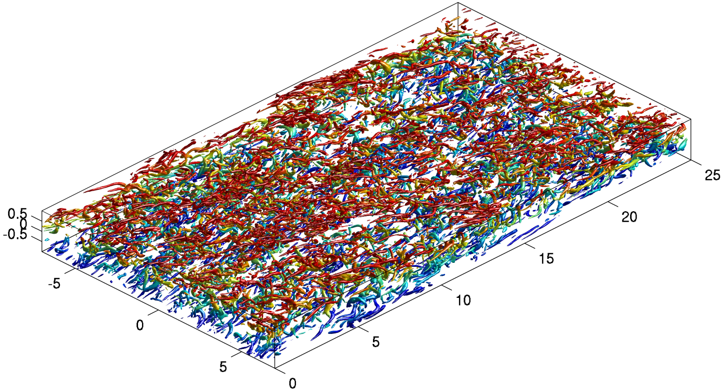

Channel flow, $Re_{\tau,c} = 180$

- Coherent vortices obtained using the **Q criterion**:

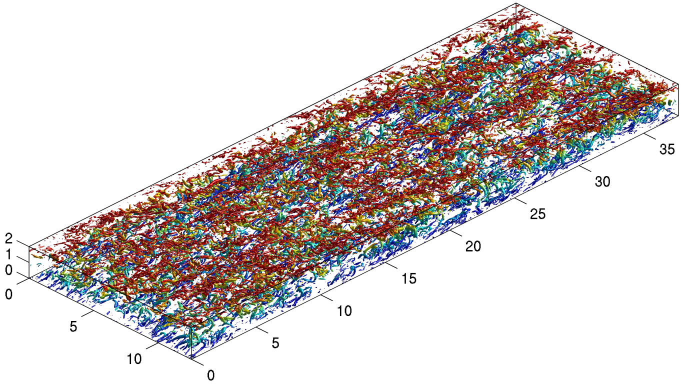

Coherent structures

- Coherent vortices are **longer in turbulent ducts flows** than in channels:

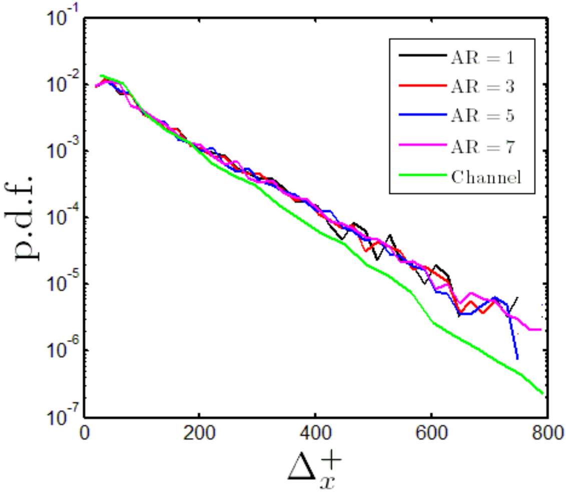

Conclusions

- For the experimental conditions studied here, **duct flow depends on the aspect ratio up to about 24**, and only becomes truly **fully-developed** for **x/H larger than 200**. Both are nearly double what we previously believed. For high Reynolds numbers, smaller values of **x/H** around 120 may be adequate.
- The **streamwise pressure gradient** does not accurately represent the skin friction along the centerline, and the spanwise pressure gradient cannot detect the three-dimensional secondary flows along the side walls. Therefore, only in **pipe flow** we can depend on axial pressure gradient for experimental determination of skin friction.
- **Best κ values**: for **ZPG boundary layer it is 0.38**, for **high-AR duct flow it is 0.35** and for **pipe flow it is 0.39-0.4** (Superpipe Pitot data corrected for turbulence intensity) $\Rightarrow$ κ **not constant**.
- Aspect ratio dependence of wall shear explained through **DNSs of turbulent duct flows** for various aspect ratios and Reynolds numbers.
- **WALL-BOUNDED TURBULENCE RESEARCH SHOULD BE FOCUSED ON THE PIPE FLOW.** $\Rightarrow$ **CICLOPE** and **NEW DNS CODES**.

Since Ricardo finished PhD we are computing AR = 18 at Re_tau ~ 550 to match experiments